Taylor & Francis
Taylor & Francis Group

Computer Methods in Biomechanics and Biomedical Engineering

ISSN: (Print) (Online) Journal homepage: https://www.tandfonline.com/loi/gcmb20

The elastoplastic numerical model and verification by macroindentation experiment of femoral head

Jun Wang, Chen Yi, Sufang Wang, Ling Wang, Haiyou Jia, Bo Chen & Yong Huan

To cite this article: Jun Wang, Chen Yi, Sufang Wang, Ling Wang, Haiyou Jia, Bo Chen & Yong Huan (2021): The elastoplastic numerical model and verification by macroindentation experiment of femoral head, Computer Methods in Biomechanics and Biomedical Engineering, DOI: 10.1080/10255842.2021.1902510

To link to this article: https://doi.org/10.1080/10255842.2021.1902510

COMPUTER METHODS IN BIOMECHANICS AND BIOMEDICAL ENGINEERING
https://doi.org/10.1080/10255842.2021.1902510

The elastoplastic numerical model and verification by macroindentation experiment of femoral head

Jun Wang[a,b], Chen Yi[c], Sufang Wang[a,b], Ling Wang[d], Haiyou Jia[a,b], Bo Chen[a,b] and Yong Huan[a,b,e]

[a]State Key Laboratory of Nonlinear Mechanics (LNM), Institute of Mechanics, Chinese Academy of Sciences, Beijing, China; [b]School of Engineering Science, University of Chinese Academy of Sciences, Beijing, China; [c]Department of Traumatic Orthopedics, Beijing Jishuitan Hospital, Beijing, China; [d]Department of Radiology, Beijing Jishuitan Hospital, Beijing, China; [e]Beijing Key Laboratory of Engineered Construction and Mechanobiology, Beijing, China

ABSTRACT

For internal fixation of proximal femoral fractures, a screw is commonly placed into the femoral head; therefore, mechanical matching of the femoral head and screw is important. This article proposes an elastoplastic numerical model of the femoral head that takes nonlinear deformation and cancellous bone heterogeneity into account. Force–depth curves from finite element analysis based on the model were compared with those from macroindentation experiments. The maximum difference between the indentation depth shown by the finite element model and that found with macroindentation testing was 5.9%, which demonstrates that the model is valid.

ARTICLE HISTORY
Received 22 September 2020
Accepted 9 March 2021

KEYWORDS
Femoral head; indentation; finite element; biomechanics; numerical model

1. Introduction

Worldwide, proximal femoral fracture is a common occurring trauma (Cumming et al. 1997), and the number of patients with proximal femoral fracture will continue to increase as the population ages—by 2050, the number of over 60 s will exceed a fifth of the global population according to WTO. Femoral head fractures, femoral neck fractures, and intertrochanteric fractures are all classified as fractures of the proximal femur. Open reduction and internal fixation is one of the most common operative treatments for these fractures (Giannoudis et al. 2009; Yang et al. 2013; Ostrum et al. 2014; Arslan et al. 2016; Filipov et al. 2017), and the typical method of internal fixation is to drive the screw into the femoral head (Oransky et al. 2012; Elgeidi et al. 2017; Blitz et al. 2018); therefore, the ability of the femoral head to hold the screw is very important. Mechanical matching of the femoral head and fixation should be verified before surgery.

In experimental bone mechanics, methods such as compression testing with a cylindrical specimen and the tensile testing of the dumbbell specimen can be used to determine the tissue-level mechanical properties of bone (Keaveny et al. 1999; Mirzaali et al. 2016). Micro- and nanoindentation tests can be used to determine micro- and nanoscale bone properties (Hengsberger et al. 2003; Casanova et al. 2010; Cory et al. 2010), and indentation test device continue to be developed (Huang et al. 2011; Geng et al. 2019; Peng et al. 2020). Macroindentation testing is an experimental method based on micro- and nanoindentation test principles. Macroindentation testing is particularly suitable for bone mechanics research because strict experimental assumptions are not necessary. End-artifacts (Keaveny et al. 1999) from the compression of cylindrical specimens can be avoided, and the comprehensive mechanical response of the bone in the indentation area can be observed (Vidotto et al. 2017).

Numerical investigation is also used in bone mechanics research. Finite element modeling has been used to determine maximum principal compressive stresses of the medial femoral neck (Keyak et al. 1990) and to predicted hip fracture patterns in human femur (Marco et al. 2019). In many studies, cancellous bone is considered to be mostly homogeneous (Zdero et al. 2008; Farrokhi et al. 2011; Samsami et al. 2015; Meena et al. 2016), which does not match the fact that human bone has heterogeneous characteristics. In some published studies (Cody et al. 1999;

CONTACT Yong Huan huany@lnm.imech.ac.cn

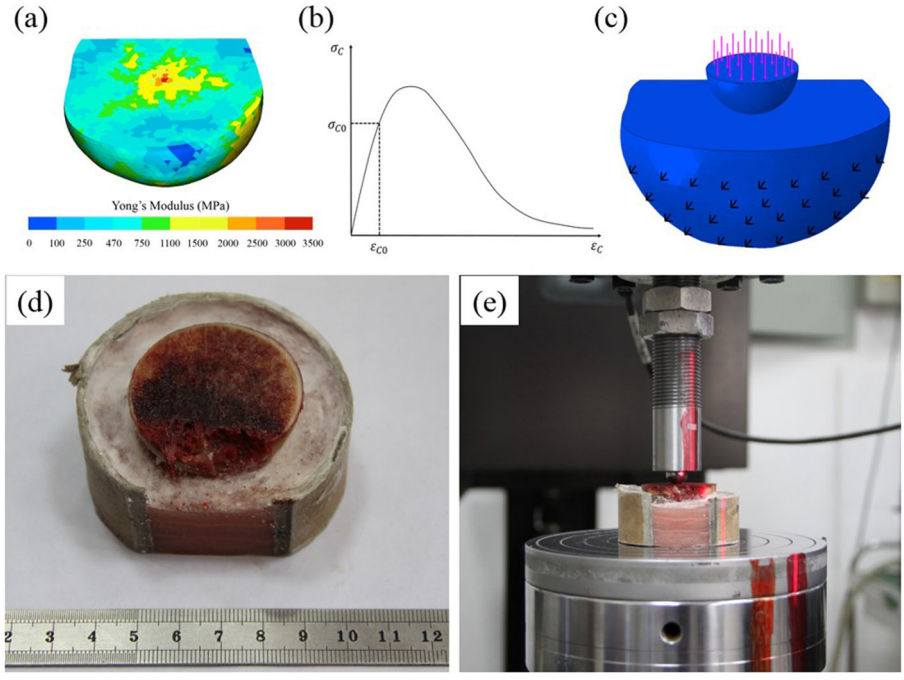

Figure 1. Numerical investigation and macroindentation experiment process.

Bessho et al. 2007; Ghosh et al. 2015), mechanical properties of femoral head were assigned to finite element models based on CT values, which reflects the heterogeneity of bone. In addition to the heterogeneity, bone plasticity after overloading should also be considered in the finite element analysis.

Therefore, we aimed to (i) establish a numerical model of the femoral head that takes into account both heterogeneity and the elastoplasticity of bone; (ii) verify the numerical model using macroindentation experiments; and (iii) use the numerical model in a clinical application, namely screw selection for proximal femoral fracture.

2. Method

This study obtained ethics approval from the Ethics Committee of Beijing Jishuitan Hospital (approval number is 201703-17).

2.1. Elastoplastic numerical model of the femoral head

The femoral head model was established based on numerical simulation methods, which can be used to describe the heterogeneity of bone and the mechanical behavior of bone after overloading.

The three-dimensional geometric model of femoral head was constructed from computed tomography (CT) data in DICOM format using the Mimics Innovation Suite (Materialise, Leuven, Belgium). Tetrahedral elements were then generated, overlapping the voxels to allow material properties of elements to be assigned according to the CT value of the voxels, as shown in Figure 1(a). However, the relationship between CT value and Young's modulus is site-dependence (Morgan et al. 2003); therefore, the relationship formula should be determined based on the specific anatomy being modeled. The relationship between CT value and Young's modulus of femoral head obtained from experiments data (Rho et al. 1995) was

$$E = 0.01*(131 + 1.067CT)^{1.86}, \quad (1)$$

where CT is CT value in Hu (Hounsfield Unit); and E is the Young's modulus expressed in megapascal (MPa). The Poisson's ratio is set to 0.3 and the yield strain ε_c is set to 0.85% (Morgan and Keaveny 2001). A typical compression stress–strain curve for human trabecular bone is shown in Figure 1(b) (Zhang et al. 2010; Morgan et al. 2018). Studies (Morgan and Keaveny 2001; Nazarian et al. 2006) have shown that the yield strain depends only on the anatomical part and is independent of the elastic modulus, the yield strain is more suitable as the yield criterion.

2.2. Macroindentation experiment

For comparison with the finite element analysis, a macroindentation experiment was conducted. A fresh

femoral head displaced during an operation was used as the specimen. The patient is a 90-year-old woman with no history of prior injury or bone disease. The entire experimental process, including sample preparation and testing, took no more than 5 hours, which ensured the bone specimen remained fresh. Study (Mittra et al. 2006) shows that experiments will have different results if indentations are performed in different time periods.

The femoral head had a diameter of 41.3 mm. The sample was sawn in half along the cross-section, then fixed on a cylindrical polyvinyl chloride support filled with solidified dental powder, as shown in Figure 1(d). This sample support can effectively prevent the sample from shaking during the loading and unloading experiment process.

The experiment was conducted on material testing machine (MTS 810, Minneapolis, MN, USA), as shown in Figure 1(e). Because the sample was incomplete, an indenter with a diameter of 12 mm was chosen such that it was small enough that the indentation would not be affected by the sample boundary, but large enough to cause indentation that would reflect material heterogeneity.

The experiment was performed at a temperature of 22 °C with a humidity of 35%. The sample was first subjected to uniform compressive loading up to 600 N then unloaded to 0 N at a rate of 0.5 mm/min. Force and indenter depth data during the experiment were exported for later analysis.

2.3. Numerical simulation

The CT data of the macroindentation experiment sample was used for numerical simulation geometric modeling. The femur was scanned before testing with a multi-slice clinical CT-scanner (TOSHIBA aquilion 64, Tokyo, Japan) using clinical settings (pixel size: 0.976 mm, slice thickness: 1 mm, 120 kVp, 250 mA, FOV 499.71 mm, Std/BONE).

The numerical model was divided into 10 parts (Figure 1(a)) according to CT value, and different mechanical properties were defined in each part, so that the calculations were simplified while retaining the heterogeneity in the numerical model that was similar to that of the human femoral head. Because the CT value of the bone is represented by the grayscale value of the pixel in CT image while in the finite element analysis, the mechanical properties of the material are represented by the deformation of the element, any changes in element size will cause the average grayscale value of the element to change, which affects the strain distribution within the model. The element size was set to 1.3 mm, and the specific analysis process to account for change in size can be found in the Appendix.

To further simplify the simulation, the indenter was modeled as a hemisphere with a diameter of 12 mm. The indenter was considered to be a quasi-rigid body with a Young's modulus of 220 GPa and Poisson's ratio of 0.3. The interaction between the indenter and femoral head was set to surface-to-surface contact, and the tangential friction coefficient was set to 0.42 (Goffin et al. 2013). Elements in the contact area were properly refined. The numerical calculation model is shown in Figure 1(c).

The model simulated the mechanical behavior of the human femoral head under the experimental conditions. The distributions of stress and strain within the femoral head and the change in indentation depth were observed. Curves representing indentation displacement corresponding to load were created.

3. Results

3.1. Numerical simulation results

Figure 2 shows the stress distributions and the corresponding indentation depth. The maximum indentation depth was 1.13 mm and the maximum von Mises stress is 13.0 MPa at the peak load; the maximum indentation depth and von Mises stress after completely unloading were 0.98 mm and 13.0 MPa, respectively. Because of the plasticity and softening of the bone, there was still a large residual stress after unloading.

The force–depth curves for the macroindentation experiments and finite element simulation is shown in Figure 3. The maximum difference between the elastoplastic numerical simulation and the experimental indentation depths is 5.9%; the maximum difference between indentation depth in the experiment and that of the numerical simulation that did not take into account plasticity and the softening behavior of the femoral head is 11.3%. That is, the resultant force–depth curves of the experiment and the elastoplastic simulation were more similar, which demonstrates that the numerical model is appropriate.

3.2. The results of a clinical application example

To illustrate the clinical significance of this femoral head simulation model, a numerical simulation to choose fixation type using this model was conducted.

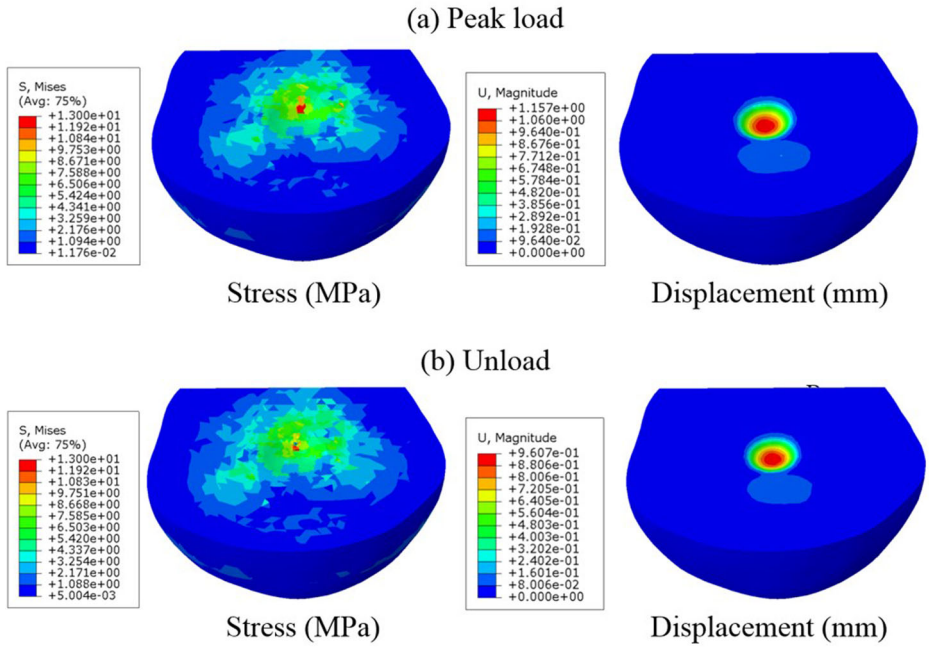

Figure 2. The von Mises stress and displacement distributions of the numerical simulation (a) at peak load and (b) after unloading.

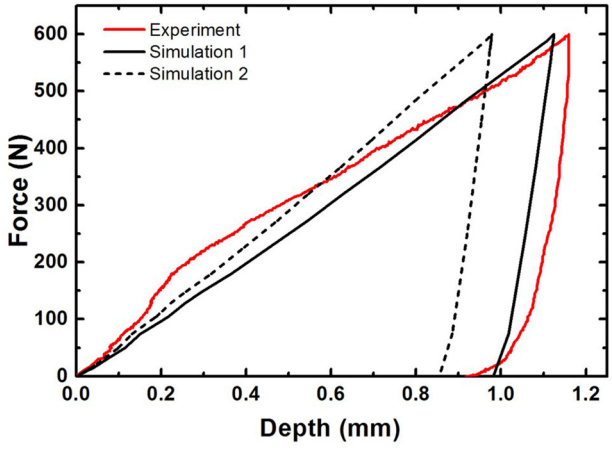

Figure 3. Comparison between macroindentation experiment and FE simulation results. The solid red line is the experimental result, the solid black line is simulation 1, which is the numerical simulation with elastoplastic model, and the broken black line is simulation 2, which is the numerical simulation that did not take plasticity and the softening behavior of femoral head into account.

This could provide a basis for clinical personalized treatment.

For intertrochanteric fractures, proximal femoral nail antirotation (PFNA) and dynamic hip screw (DHS) are two commonly used clinical internal fixation systems. In these two types of fixation systems, head fixation plays a major role in providing stability. The PFNA system uses a compression screw, whereas a helical blade is used in the DHS system, as shown in Figure 4(a). There are advantages and disadvantages to both systems, but choosing the most suitable fixations method can effectively reduce the likelihood of failure and reduces the pain of patients after surgery.

To conduct a numerical simulation to compare the fixation effects of the two head fixation systems, four volunteers' data were used (Table 1). To compare the ability of the femoral head to hold screws, models of the femoral head–compression screw and the femoral head–helical blade model were established, and 700 N, 1400 N, and 2100 N loads were applied to both models (Figure 4(a)). In the simulation, the tail of the screw was constrained, and the load was distributed on the top of the femoral head. For comparison, the volume of elements whose strain exceeds 0.85% was calculated as a parameter, reflecting the volume of plastic deformation of the cancellous bone when stressed. The volume of the plastic deformation changed with load; the results are summarized in Figure 4(b).

In Figure 4(b), the volume–force curves, where V1 represents the volume of plastically deformed elements in a femoral head fixed with the compression screw, and V2 represents the volume of plastically deformed elements in a femoral head fixed with the helical blade, show how volume increases with increasing load. The greater the plastic deformation of the bone, the more likely it is that the screw will loosen, which reflects poor fixation. The mechanical effects of compression screw and helical blade fixation

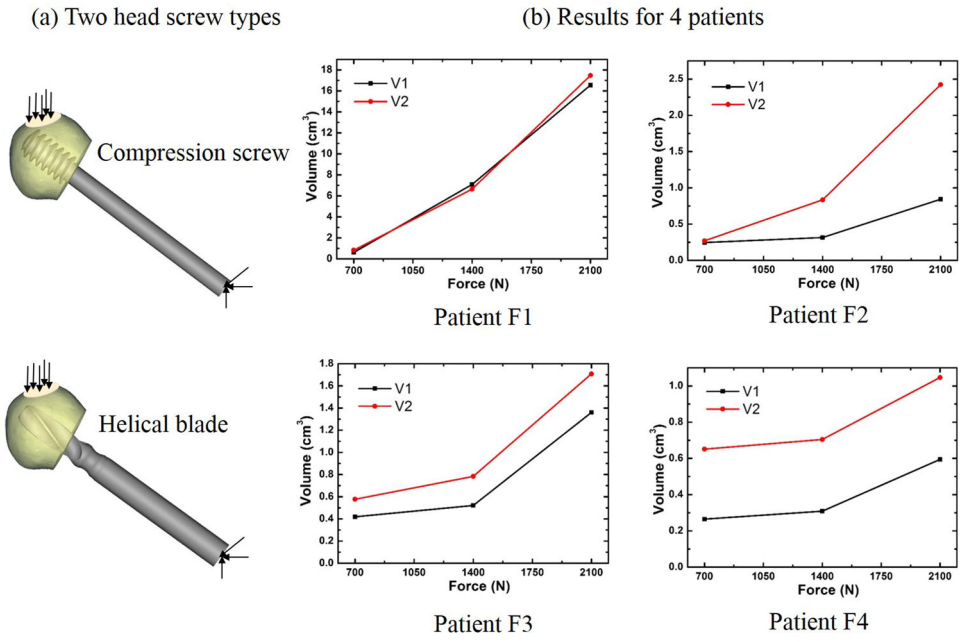

Figure 4. Comparison of the fixation effects of different screws. (a) Images of the models show the two types of fixation screws, and (b) curves show resulting deformation from applied loads.

Table 1. Volunteers' femoral head CT information.

Sample	Gender	Age	Grayscale value of bone in the screwed area (Hu)
F1	Female	88	104
F2	Female	78	162
F3	Male	86	275
F4	Female	67	228

are similar for patient F1. For patient F2, when the load is small, the effects of the two types of fixation are similar; with increased load, the damage to the bone caused by the helical blade significantly increases, whereas the compression screw appears to perform better under the corresponding load. For patients F3 and F4, no matter which load, the mechanical effect of the compression screw is better than that of the helical blade. By relating these results and the grayscale value of bone in the surrounding area (the relevant data are in Table 1), we concluded that for patients with more severe osteoporosis, the difference between the mechanical effects of the two types of fixation is not obvious, and for patients with low bone loss, compression screws are better.

4. Discussion

An elastoplastic numerical model suitable for femoral head research was established, a macroindentation test and finite element simulations based on the model were performed to verify the model. The elastoplastic numerical model reflects the heterogeneity of the mechanical properties of the femoral head and takes into account mechanical behavior after overloading. By comparing the results of the finite element simulation and the experiment, we found that the force–depth curves obtained for the two methods showed similar results, with a maximum indentation depth difference of only 5.9%. If the plasticity and softening behavior of the femoral head are not taken into account, the maximum difference is 11.3%.

To illustrate the clinical significance, we applied the simulation method to the selection of proximal internal fixation type. A model of each patient's femoral head is used to select the appropriate type of head fixation for the individually. The results show that, for patients with severe osteoporosis, there is not much difference between the fixation effects of compression screws and helical blades, while for patients with less bone loss, compression screws are better. This method has the potential to be used flexibly in clinical application, according to specific problems such as assessing the risk of surgery or choosing a surgical plan.

Acknowledgements

The authors would like to thank Professor Jie Wei for his support of the project.

Disclosure statement

The authors declare no conflict of interest.

Ethical approval

This study obtained ethical approval by Ethics Committee of Beijing Jishuitan Hospital. The ethical approval number is 201703-17.

Funding

This work is supported by the National Natural Science Foundation of China (Grant number 11972037).

References

Arslan A, Utkan A, Koca TT. 2016. Results of a compression pin alongwith trochanteric external fixation in management of high risk elderly intertrochanteric fractures. Indian J Orthop. 50(6):636–640.

Bessho M, Ohnishi I, Matsuyama J, Matsumoto T, Imai K, Nakamura K. 2007. Prediction of strength and strain of the proximal femur by a CT-based finite element method. J Biomech. 40(8):1745–1753.

Blitz AM, Northcutt B, Shin J, Aygun N, Herzka DA, Theodros D, Goodwin CR, Lim M, Seeburg DP. 2018. Contrast-enhanced CISS imaging for evaluation of neurovascular compression in trigeminal neuralgia: improved correlation with symptoms and prediction of surgical outcomes. AJNR Am J Neuroradiol. 39(9):1724–1732.

Casanova R, Moukoko D, Pithioux M, Pailler-Mattéi C, Zahouani H, Chabrand P. 2010. Temporal evolution of skeletal regenerated tissue: what can mechanical investigation add to biological? Med Biol Eng Comput. 48(8): 811–819.

Cody DD, Gross GJ, Hou FJ, Spencer HJ, Goldstein SA, Fyhrie DP. 1999. Femoral strength is better predicted by finite element models than QCT and DXA. J Biomech. 32(10):1013–1020.

Cory E, Nazarian A, Entezari V, Vartanians V, Müller R, Snyder BD. 2010. Compressive axial mechanical properties of rat bone as functions of bone volume fraction, apparent density and micro-CT based mineral density. J Biomech. 43(5):953–960.

Cumming RG, Nevitt MC, Cummings SR. 1997. Epidemiology of hip fractures. Epidemiol Rev. 19(2): 244–257.

Elgeidi A, Negery AE, Abdellatif MS, Moghazy NE. 2017. Dynamic hip screw and fibular strut graft for fixation of fresh femoral neck fracture with posterior comminution. Arch Orthop Traum Su. 137(10):1–7.

Farrokhi S, Keyak JH, Powers CM. 2011. Individuals with patellofemoral pain exhibit greater patellofemoral joint stress: a finite element analysis study. Osteoarthritis Cartilage. 19(3):287–294.

Filipov O, Stoffel K, Gueorguiev B, Sommer C. 2017. Femoral neck fracture osteosynthesis by the biplane double-supported screw fixation method (BDSF) reduces the risk of fixation failure: clinical outcomes in 207 patients. Arch Orthop Trauma Surg. 137(6):779–788.

Geng YQ, Wang JQ, Zhang JR, Cai JX, Yan YD. 2019. A probe-based forcecontrolled nanoindentation system using an axisymmetric four-beam spring. Precis Eng. 56: 530–536.

Ghosh R, Pal B, Ghosh D, Gupta S. 2015. Finite element analysis of a hemi-pelvis: the effect of inclusion of cartilage layer on acetabular stresses and strain. Comput Methods Biomech Biomed Eng. 18(7):697–710.

Giannoudis PV, Kontakis G, Christoforakis Z, Akula M, Tosounidis T, Koutras C. 2009. Management, complications and clinical results of femoral head fractures. Injury. 40(12):1245–1251.

Goffin JM, Pankaj P, Simpson AH. 2013. The importance of lag screw position for the stabilization of trochanteric fractures with a sliding hip screw: a subject-specific finite element study. J Orthop Res. 31(4):596–600.

Hengsberger S, Enstroem J, Peyrin F, Zysset P. 2003. How is the indentation modulus of bone tissue related to its macroscopic elastic response? A validation study. J Biomech. 36(10):1503–1509.

Huang H, Zhao H, Mi J, Yang J, Wan S, Yang Z, Yan J, Ma Z, Geng C. 2011. Experimental research on a modular miniaturization nanoindentation device. Res Sci Instrum. 82(9):256.

Keaveny TM, Wachtel EF, Kopperdahl DL. 1999. Mechanical behavior of human trabecular after overloading bone. J Orthop Res. 17 (3):346–353.

Keyak JH, Meagher JM, Skinner HB, Mote CD. Jr 1990. Automated three-dimensional finite element modelling of bone: a new method. J Biomed Eng. 12(5):389–397.

Marco M, Eugenio G, Ramón C-RJ, Henar MM, Ricardo L-G. 2019. Numerical modelling of hip fracture patterns in human femur. Comput Methods Programs Biomed. 173:67–75.

Meena VK, Kumar M, Pundir A, Singh S, Goni V, Kalra P, Sinha RK. 2016. Musculoskeletal-based finite element analysis of femur after total hip replacement. Proc Inst Mech Eng H. 230(6):553–560.

Mirzaali MJ, Schwiedrzik JJ, Thaiwichai S, Best JP, Michler J, Zysset PK, Wolfram U. 2016. Mechanical properties of cortical bone and their relationships with age, gender, composition and microindentation properties in the elderly. Bone. 93:196–211.

Mittra E, Akella S, Qin YX. 2006. The effects of embedding material, loading rate and magnitude, and penetration depth in nanoindentation of trabecular bone. J Biomed Mater Res. 79A(1):86–93.

Morgan EF, Bayraktar HH, Keaveny TM. 2003. Trabecular bone modulus-density relationships depend on anatomic site. J Biomech. 36(7):897–904.

Morgan EF, Keaveny TM. 2001. Dependence of yield strain of human trabecular bone on anatomic site. J Biomech. 34(5):569–577.

Morgan EF, Unnikrisnan GU, Hussein AI. 2018. Bone mechanical properties in healthy and diseased states. Annu Rev Biomed Eng. 20:119–143.

Nazarian A, Stauber M, Zurakowski D, Snyder BD, Müller R. 2006. The interaction of microstructure and volume fraction in predicting failure in cancellous bone. Bone. 39(6):1196–1202.

Oransky M, Martinelli N, Sanzarello I, Papapietro N. 2012. Fractures of the femoral head: a long-term follow-up study. Musculoskelet Surg. 96(2):95–99.

Ostrum RF, Tornetta P, Watson JT, Christiano A, Vafek E. 2014. Ipsilateral proximal femur and shaft fractures treated with hip screws and a reamed retrograde intramedullary nail. Clin Orthop Relat Res. 472(9):2751–2758.
Peng GJ, Xu FL, Chen JF, Hu YH, Wang HD, Zhang TH. 2020. A cost-effective voice coil motor-based portable micro-indentation device for in situ testing. Measurement. 165:108105.
Rho JY, Hobatho MC, Ashman RB. 1995. Relations of mechanical properties to density and CT numbers in human bone. Med Eng Phys. 17(5):347–355.
Samsami S, Saberi S, Sadighi S, Rouhi G. 2015. Comparison of three fixation methods for femoral neck fracture in young adults: experimental and numerical investigations. J Med Biol Eng. 35(5):566–579.
Vidotto VT, Batista NA, Mariolani JRL, Belangero WD. 2017. Quantitative evaluation of experimental bone regeneration using indentation tests. Acta Ortop Bras. 25(2):71–76.
Yang YH, Wang YR, Jiang SD, Jiang LS. 2013. Proximal femoral nail antirotation and third-generation Gamma nail: which is a better device for the treatment of intertrochanteric fractures? Singapore Med J. 54(8):446–450.
Zdero R, Olsen M, Bougherara H, Schemitsch EH. 2008. Cancellous bone screw purchase: a comparison of synthetic femurs, human femurs, and finite element analysis. Proc Inst Mech Eng H. 222(8):1175–1183.
Zhang J, Michalenko MM, Kuhl E, Kuhl E, Ovaert TC. 2010. Characterization of indentation response and stiffness reduction of bone using a continuum damage model. J Mech Behav Biomed Mater. 3(2):189–202.

Appendix

The pixel size and slice thickness of the CT used in this paper are approximately 1 mm; therefore, the size of the element should be close to 1 mm. To find the most suitable element size, six identical femoral head models from the same CT data were established, the element sizes of these six femoral heads were set to 0.4 mm, 0.7 mm, 1.0 mm, 1.3 mm, 1.6 mm, and 1.9 mm, respectively, and the elements of each femoral head model was divided into 10 parts according to the CT value. The proportion of the element volume in each part to the total femoral head model volume was calculated. The results are shown in Table A1.

The 'voxel group' was the proportion of the voxel volume of each part to the total volume of the femoral head model. The overall difference between each group and the voxel group, was calculate as follows:

$$\sigma_j = \sum_{i=1}^{10} \left| k_{ji} - \hat{k}_i \right|, \tag{A1}$$

where j represents different element size groups; σ_j represents the overall difference for group j; k_{ji} represents the proportion of the element volume in part i for group j, and $\hat{k}_i$ represents the proportion of the element volume in part i for the voxel group.

When the element size is 1.3 mm, the overall difference is the smallest, as shown in Figure A1. That is to say, in this study, when the element size is set to 1.3 mm, meshing has little effect on the material property distributions.

Table A1. Relative proportion of the element volume in each part for different element sizes.

	Proportion (%)						
Element size	Voxel	0.4 mm	0.7 mm	1.0 mm	1.3 mm	1.6 mm	1.9 mm
Part 1	1.29	1.74	1.54	1.36	1.03	1.12	1.06
Part 2	11.97	15.63	15.13	14.05	10.87	11.54	10.45
Part 3	25.95	30.00	29.79	28.98	26.15	26.56	25.06
Part 4	26.76	27.21	27.45	27.60	27.42	27.33	26.56
Part 5	19.81	17.32	17.73	18.63	20.76	20.62	21.09
Part 6	9.41	5.67	5.87	6.55	9.57	9.10	10.65
Part 7	3.40	2.01	2.06	2.28	3.08	2.80	3.57
Part 8	1.17	0.39	0.41	0.49	0.94	0.79	1.28
Part 9	0.21	0.02	0.02	0.05	0.17	0.14	0.26
Part 10	0.02	0.01	0.00	0.00	0.01	0.01	0.02

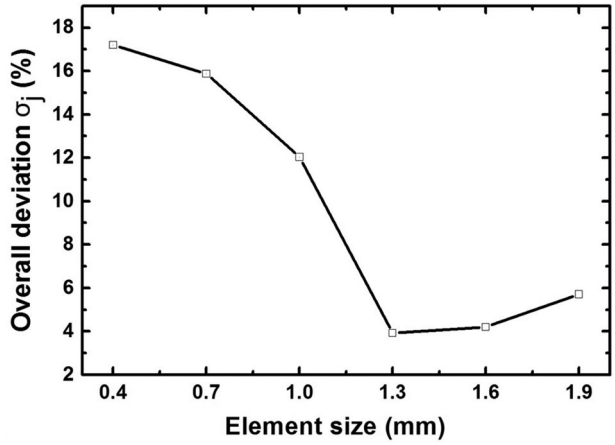

Figure A1. Effect of element size on material property assignment.